appear in Proceed of the 1976 Division of Particles
d Fields, American Physical Society Meeting, Brookhaven, Oct., 1976

FERMILAB

FEB 25 1977

LIBRARY

CONF-76-109-E
E-0002

E2B

Multiparticle Processes at Fermilab Energies

J. Whitmore
Department of Physics
Michigan State University, E. Lansing, Michigan 48824*

Abstract

A summary is given of charged particle multiplicity moments up to Fermilab energies and comparisons are made between the distributions obtained in different reactions. Inclusive single $\pi^{\pm}$ production is discussed in terms of the energy dependence observed in the central and target fragmentation regions. New data are presented on the energy and multiplicity dependence of semi-inclusive π^- production at 90° CM. Two-particle rapidity correlations are studied as a function of $\sqrt{s}$ and it is found that the three-particle density may be expressed in terms of one- and two-particle densities. New data on charged particle production from 100 GeV/c $p^{\pm}p$, $\pi^{\pm}p$ interactions are presented as the sums and differences of the four reactions and the rapidity distributions for proton and pion fragmentation and central pionization and annihilation are obtained.

I. Charged Particle Multiplicities

Figure 1 shows the charged multiplicity moments, $\langle n_c \rangle$, $\langle n_c \rangle/D$, and f_2^{cc}, for all available data[1/] as a function of the incident laboratory momentum. At the higher energies, it appears that the values for the reactions Ap and $\bar{A}p$ are approaching each other. However, on closer examination, the negative beam particle reactions may be seen to produce slightly higher charged particle multiplicities. A recent summary[2/] of fits to $\langle n_c \rangle$, the average charged particle multiplicity, as a function of s is shown

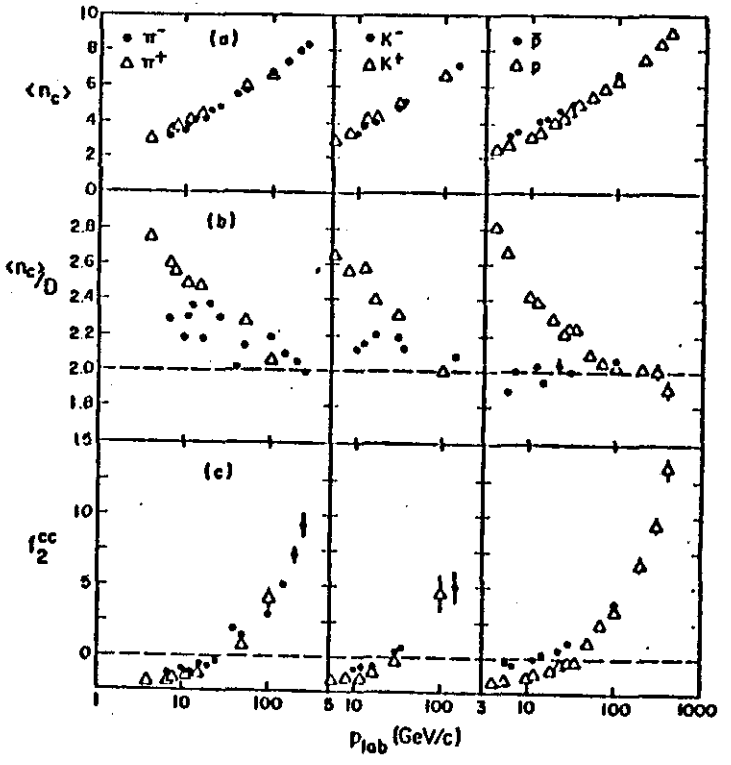

Fig. 1. Multiplicity moments as a function of the beam momentum for $\pi^{\pm}p$, $K^{\pm}p$, and $p^{\pm}p$ interactions. (a) Average charged multiplicity, (b) Ratio of the average charged multiplicity to dispersion, and (c) $f_2^{cc}=\langle n_c(n_c-1)\rangle-\langle n_c\rangle^2$.

in Fig. 2. The results[2/] of the fits are shown in Table I. It is interesting to note that the coefficient of the $\ln s$ term, B, appears to be independent of the incident beam particle suggesting that at higher s values $\langle n_c \rangle$ may be independent of the incident channel.

While Figures 1 and 2 suggest that, to a first approximation, the charged multiplicity distribution does not depend on the nature of the beam, it is informative to study the small, but significant, differences

TABLE I

Fits of Average Charged-Particle Multiplicities to the Form
$A + B \ln s + C \ln s/s^{1/4}$

Channel	Parameters		
	A	B	C
pp	2.68 ± 0.42	1.45 ± 0.02	-2.68 ± 0.33
$\bar{p}p$	5.17 ± 0.56	1.32 ± 0.04	-3.76 ± 0.48
K^+p	2.42 ± 0.35	1.43 ± 0.07	-2.19 ± 0.39
K^-p	0.77 ± 1.64	1.47 ± 0.11	-1.22 ± 1.34
π^+p	3.02 ± 0.96	1.32 ± 0.10	-2.11 ± 0.86
π^-p	0.33 ± 0.36	1.43 ± 0.01	-0.68 ± 0.23
γp	1.42 ± 1.02	1.13 ± 0.58	-0.64 ± 1.80
e^+e^-	1.47 ± 0.89	0.67 ± 0.17	0.49 ± 0.98

that do exist between the various reactions at fixed incident beam momentum. Figure 3 shows a comparison of the data from 400 GeV/c pp[3] and 360 GeV/c π^-p[4] interactions. The form of this plot is motivated by a comparison with a Poisson distribution in n_-:

$$\sigma_{n_-} = \sigma_{inel} \langle n_- \rangle^{n_-} e^{-n_-}/n_-! \qquad (1)$$

which predicts that $\ln(n_- \sigma_n) \propto n_-$. Figure 3 suggests that the upward curvature is much stronger for the pp data than for the π^-p data. The differences between πp, Kp and pp data at 100 GeV/c are shown clearly in Fig. 4 where σ_n is plotted versus n.[1] For $n \lesssim 10$, the differences are mainly a reflection of the differences in total cross section. However, for $n \gtrsim 12$ we see that the cross sections are insensitive to the beam particle, with the notable exception of the $\bar{p}p$ reaction where the high multiplicity cross sections are significantly larger than those found in

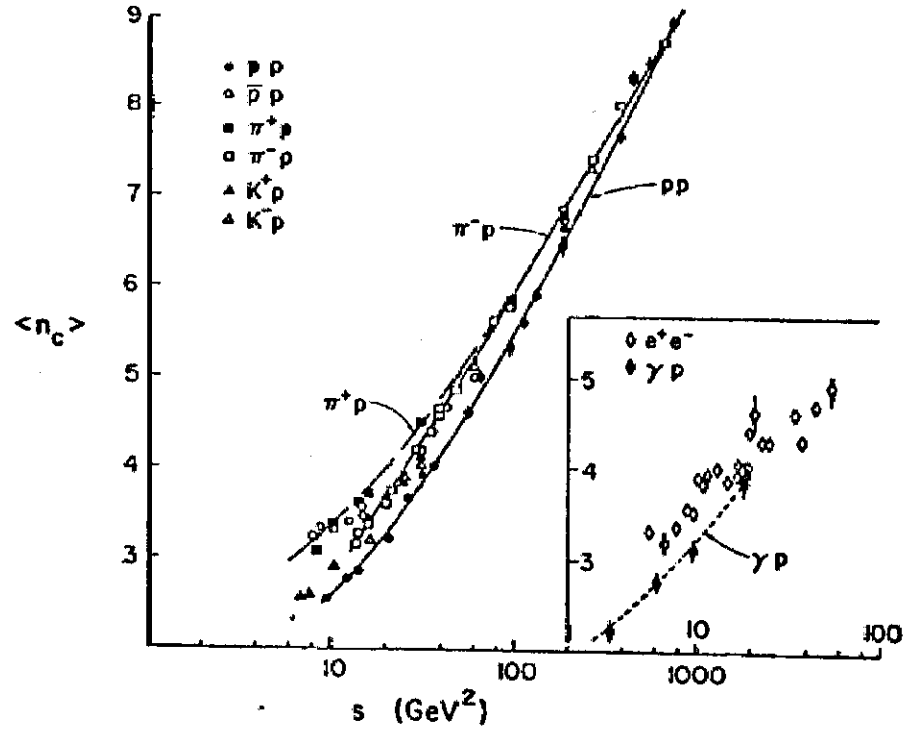

Fig. 2. Average charged multiplicity as a function of s for all available data. The curves represent fits with the parameters given in Table I.

the other four reactions. It is tempting to ascribe the larger $\bar{p}p$ cross sections to the baryon-annihilation process.[5]

II. Inclusive Charged Particle Production

Some new inclusive data from π^-p interactions are shown[1] in Fig. 5 where the invariant cross section is plotted as a function of the Feynman x variable, $x = 2p_L^*/\sqrt{s}$. The two dominant features of Fig. 5 are that

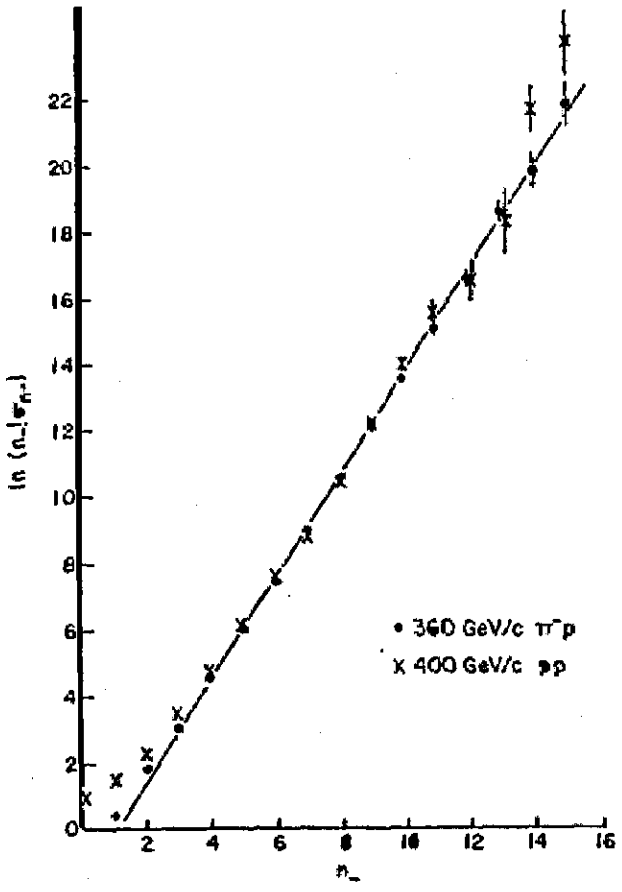

Fig. 3. $\ln(n_{-}\sigma_{n_{-}})$ versus n_{-} for 400 GeV/c pp and 360 GeV/c $\pi^{-}p$ interactions.

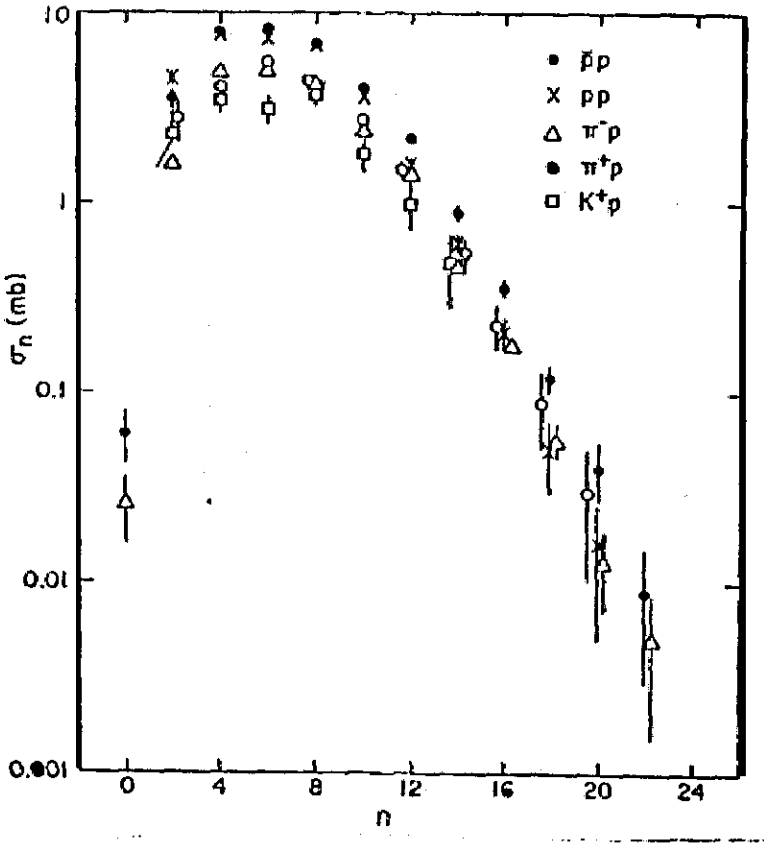

Fig. 4. Inelastic topological cross sections for $p^{\pm}p$, $\pi^{\pm}p$ and $K^{+}p$ interactions at 100 GeV/c.

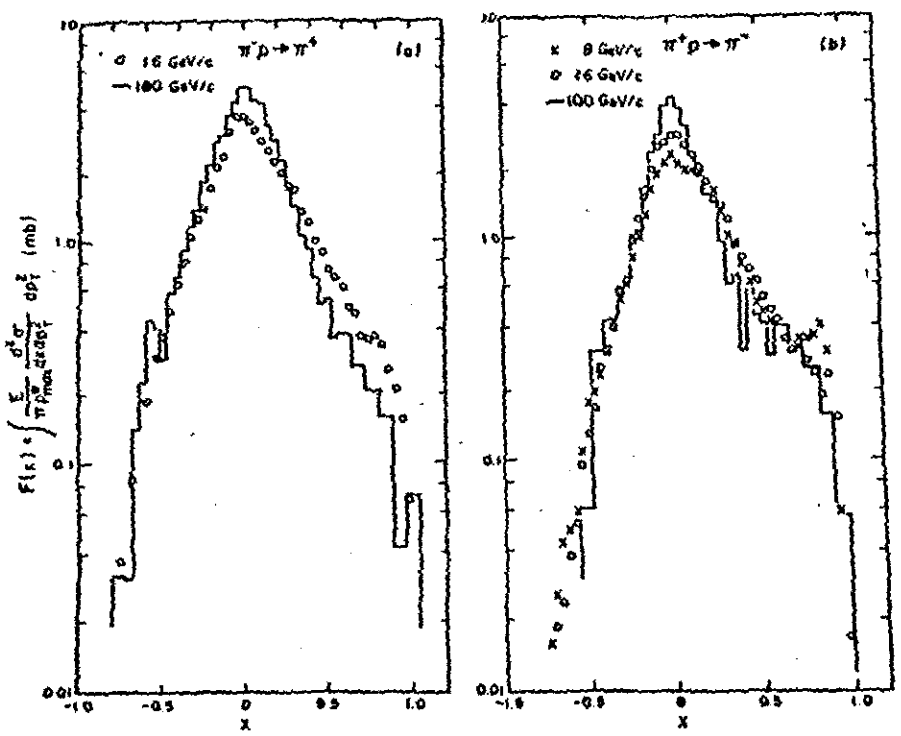

Fig. 5. Invariant cross section as a function of x for (a) $\pi^- p \to \pi^+ + X$, (b) $\pi^+ p \to \pi^- + X$.

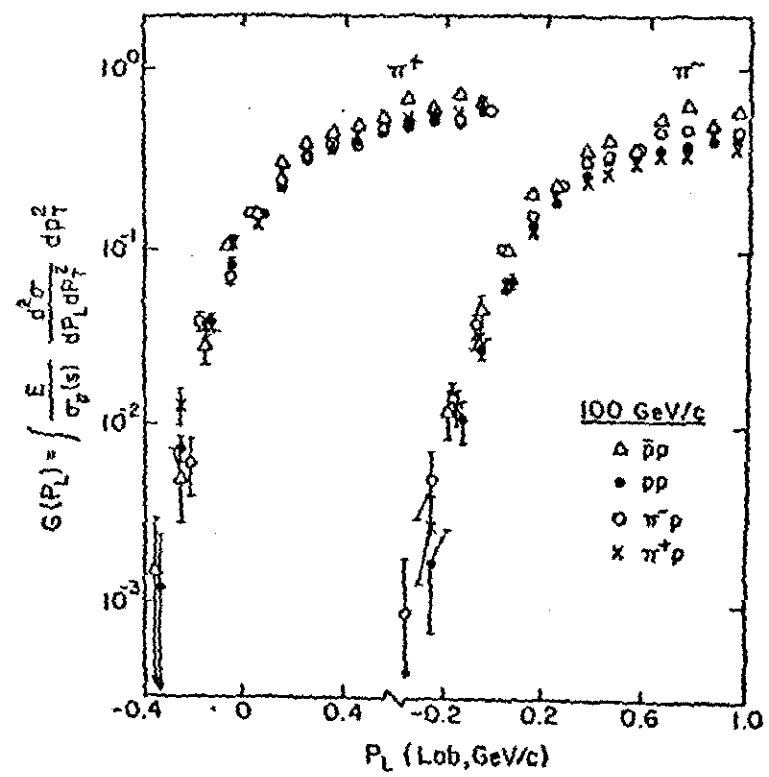

Fig. 6. Invariant cross section, normalized to the Pomeron contribution $\sigma_p(s)$, as a function of the laboratory longitudinal momentum for $\pi^\pm$ production in $\pi^\pm p$, $p^\pm p$ interactions at 100 GeV/c.

(a) the cross sections in the target and beam fragmentation regions are falling as the incident momentum increases, and (b) the cross sections at $x = 0$ are increasing.

The target fragmentation region is shown in more detail in Fig. 6 where the data for $\pi^\pm$ production are compared for $\pi^\pm p$ and $p^\pm p$ interactions at 100 GeV/c as a function of the $\pi^\pm$ laboratory longitudinal momentum. Note that we have normalized to $\sigma_p(s)$ the Pomeron contribution to σ_T.[1] The eight distributions are quite similar although certain trends are observable: the $\bar{p}p$ cross sections are largest and, for π^- production, the $\pi^+ p$ data are smallest. In order to study the energy and incident channel dependence in more detail, Fig. 7 shows $\int_{-0.4}^{0.2} G(P_L)\, dP_L$ as a function of $s^{-1/2}$ for $\pi^\pm$ production. In the Fermilab energy range, it appears that all cross sections are decreasing with increasing $\sqrt{s}$ although the rate of decrease is strongly dependent upon the nature of the beam particle.

Central region $\pi^\pm$ production is summarized[1] in Fig. 8 where the cross section at CM rapidity $y^*=0$, $\frac{d\sigma}{dy}(y^*=0)$, is plotted versus $s^{-1/4}$ (as expected from Mueller-Regge theory). There are trends for the higher energy data to be less sensitive to the incident channel and for the $\bar{p}p$ and $\pi^\pm p \to \pi^\pm$ reactions to decrease from their values at low energy and to reach their smallest value in the Fermilab energy range.

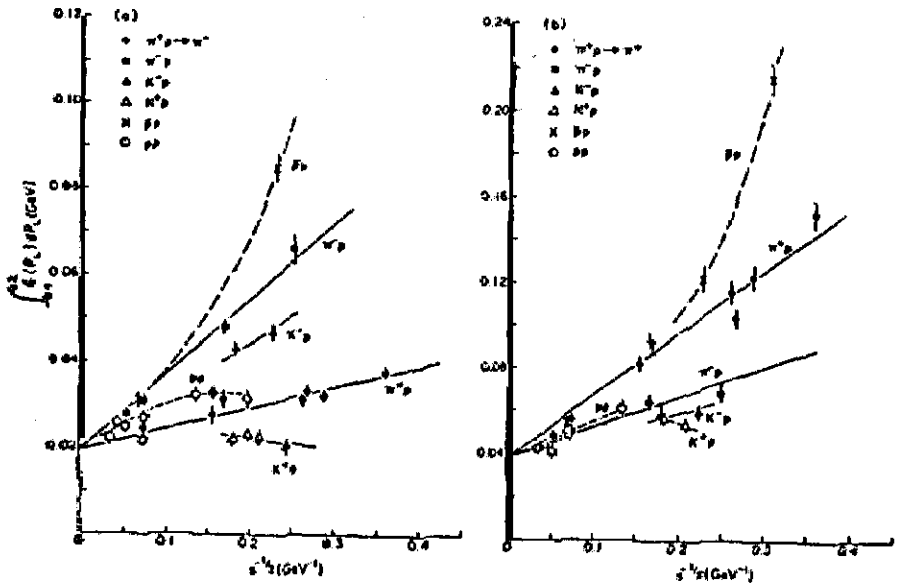

Fig. 7. Invariant cross section integrated over the proton fragmentation region as a function of $s^{-1/2}$. The curves are drawn to guide the eye.

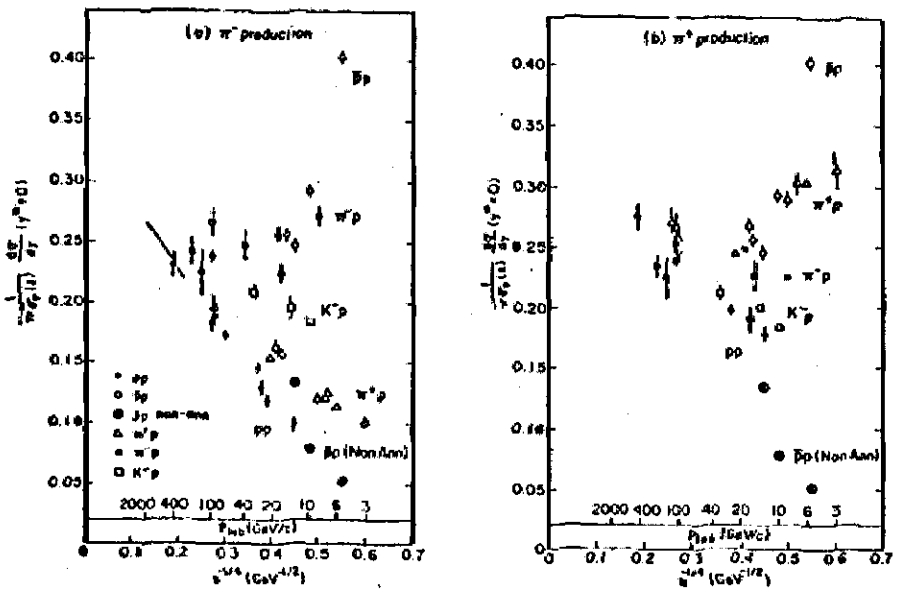

Fig. 8. Normalized invariant cross sections at y*=0 for (a) π^- and (b) π^+ production as a function of $s^{-1/4}$.

The pp central region data have recently been studied[6] semi-inclusively, i.e., as a function of n, the charged particle multiplicity of the final state. Figure 9 shows the CM rapidity distribution for π^- and charged pion production in 200 GeV/c pp interactions for different n. The two main features of this figure are (a) the dip in the center of the four-prong rapidity distribution and (b) the linear dependence on n for the π^- spectra at y*=0. Figure 10 contains a summary of the energy and n dependence of semi-inclusive π^- production at y*=0 in pp interactions. As an empirical observation we find that $F_n(0)$ may be parameterized by the form

$$F_n(o) = (-0.8 + 1.6n_- + 0.05n_-^2)/\ln(E_a^2/m_p^2). \qquad (2)$$

It is remarkable that this simple form gives such an excellent representation of these data over wide ranges in both n_- and $E_a = \sqrt{s} - 2m_p$.

III. Two- and Three-Particle Correlations

New high statistics data[7] from π^-p interactions at 200 and 360 GeV/c permit an energy dependent study of the two-particle rapidity correlation functions. Using the following single- and two-particle densities

$$\rho_1(y) = \frac{1}{\sigma_{inel}} \frac{d\sigma}{dy} \quad \text{and} \quad \rho_2(y_1,y_2) = \frac{1}{\sigma_{inel}} \frac{d^2\sigma}{dy_1 dy_2}, \qquad (3)$$

we can define an inclusive function

$$R(y_1,\Delta y) = \frac{\rho_2(y_1,y_2)}{\rho_1(y_1)\,\rho_2(y_2)} - 1 \qquad (4)$$

with $\Delta y = y_1 - y_2$. Similarly, we can define a semi-inclusive function $R_n(y_1, \Delta y)$. Figure 11 shows the inclusive R, integrated over all y_1 and n for like and unlike charge pairs for incident momenta ranging from 8 to 360 GeV/c.[7] Similarly, Fig. 12 shows $R_n^*(\Delta y) = R_n(\Delta y) + 1/n_-$ for two

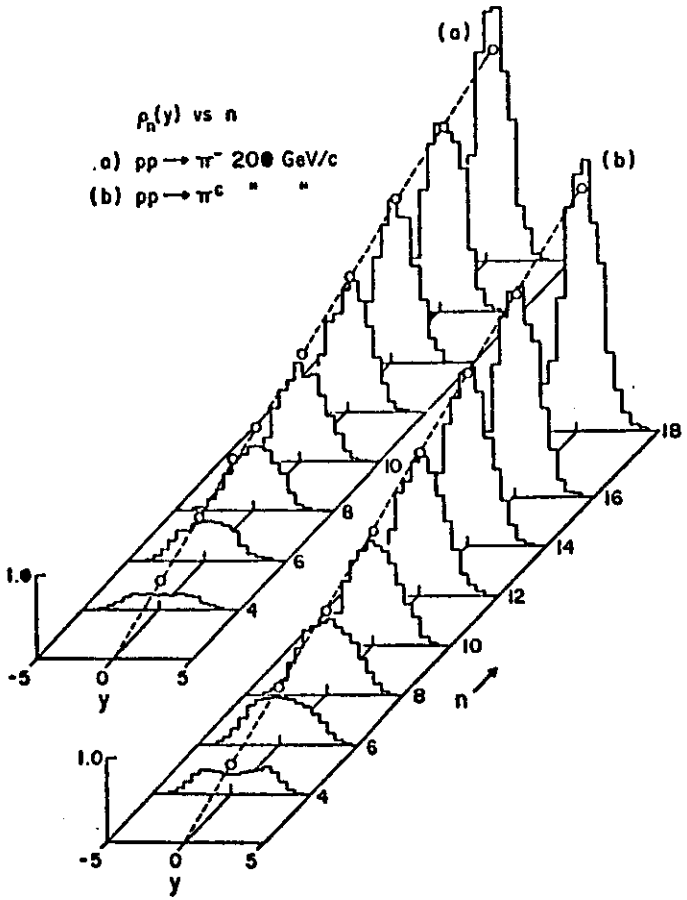

Fig. 9. Semi-inclusive single particle densities, $\rho_n = \frac{1}{\sigma_n}\frac{d\sigma_n}{dy}$, for π^- and charged pion production in 200 GeV/c pp interactions.

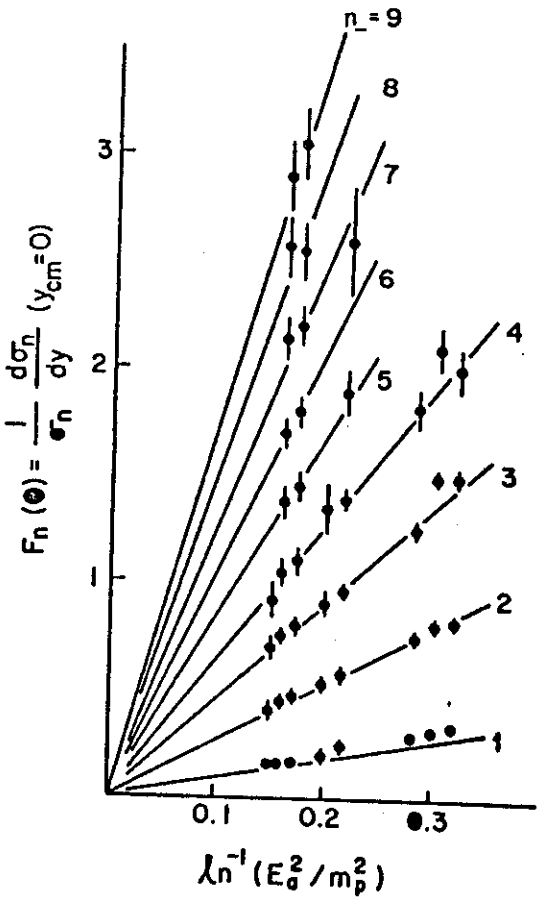

Fig. 10. $F_n(y^*=0)$ versus $\ln^{-1}(E_a{}^2/m_p{}^2)$ for various values of n_-. The solid lines are given by Eq. (2) in text.

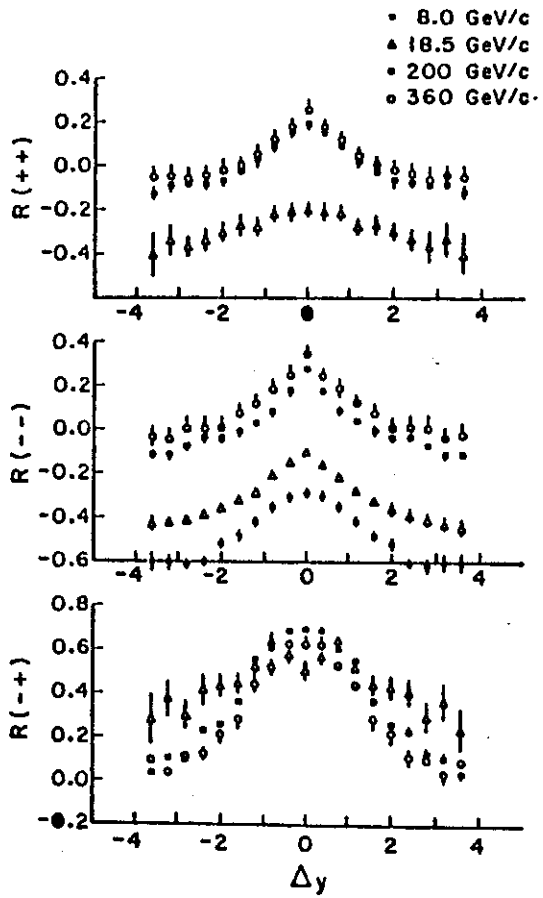

Fig. 11. Inclusive two-particle correlation function, $R(y_1,\Delta y)$, integrated over all y_1 as a function of $\Delta y = y_1 - y_2$ for particles of like and unlike charge.

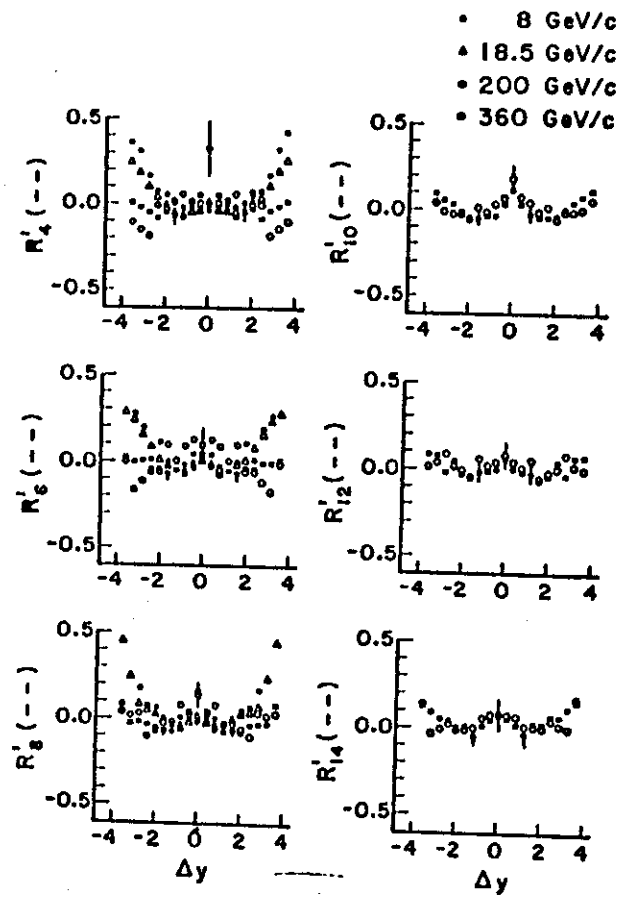

Fig. 12. Semi-inclusive two-particle correlation function, $R'_n(\Delta y) = R_n(\Delta y) + 1/n_-$, integrated over all y_1 as a function of Δy for two negatively charged particles.

negatively charged particles. In both figures short-range two-particle correlations are clearly apparent, with the value of $R(\Delta y=0)$ rising with increasing momentum and falling with increasing charged multiplicity. The energy dependence is summarized in Figure 13 where $R(\Delta y=0)$ is plotted versus $\sqrt{s}$ for the inclusive, 4-, 6-, and 8-prong data. The semi-inclusive data show a $\ln s$ dependence.

Recently, high statistics 200 GeV/c pp data have been used to investigate[8] possible three-particle correlations. With the definition of a two-particle correlation function,

$$\tilde{C}_n(i,j) = \frac{\rho_2^n(i,j)}{n(n-1)} - \frac{\rho_1^n(i)\,\rho_1^n(j)}{n^2}\,, \qquad (5)$$

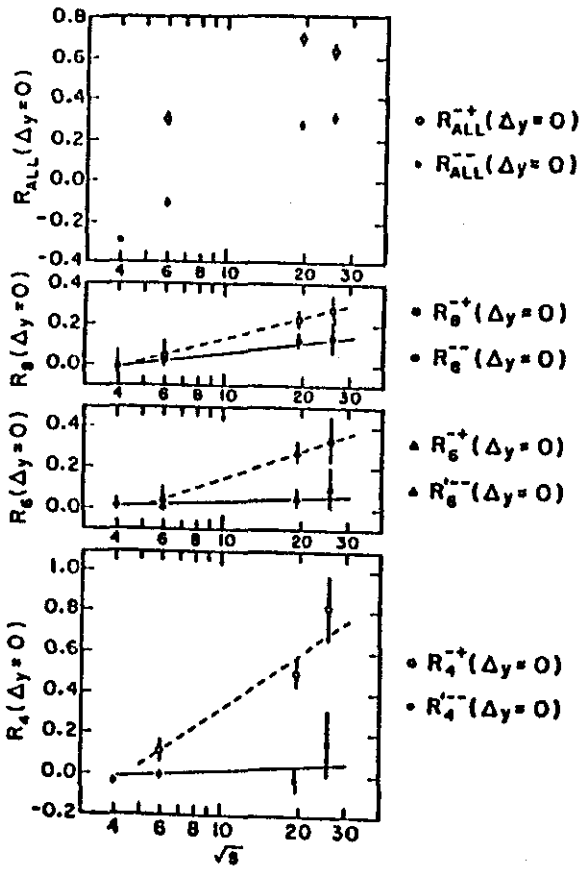

Fig. 13. Inclusive and semi-inclusive correlations at $\Delta y=0$ as a function of $\sqrt{s}$. The curves are drawn to guide the eye.

we define

$$\tilde{C}_n(1,2,3) = \frac{\rho_n(1,2,3)}{n(n-1)(n-2)} - \frac{\rho_1^n(1)\ \rho_1^n(2)\ \rho_1^n(3)}{n^3} \tag{6}$$

$$- \frac{1}{n}\,[\rho_1^n(1)\ \tilde{C}_n(2,3) + \rho_1^n(2)\ \tilde{C}_n(3,1) + \rho_1^n(3)\ \tilde{C}_n(1,2)].$$

We find experimentally that $\tilde{C}_n(1,2,3)$ is approximately zero. This suggests that the three-particle density may be expressed in terms of one- and two-particle densities:

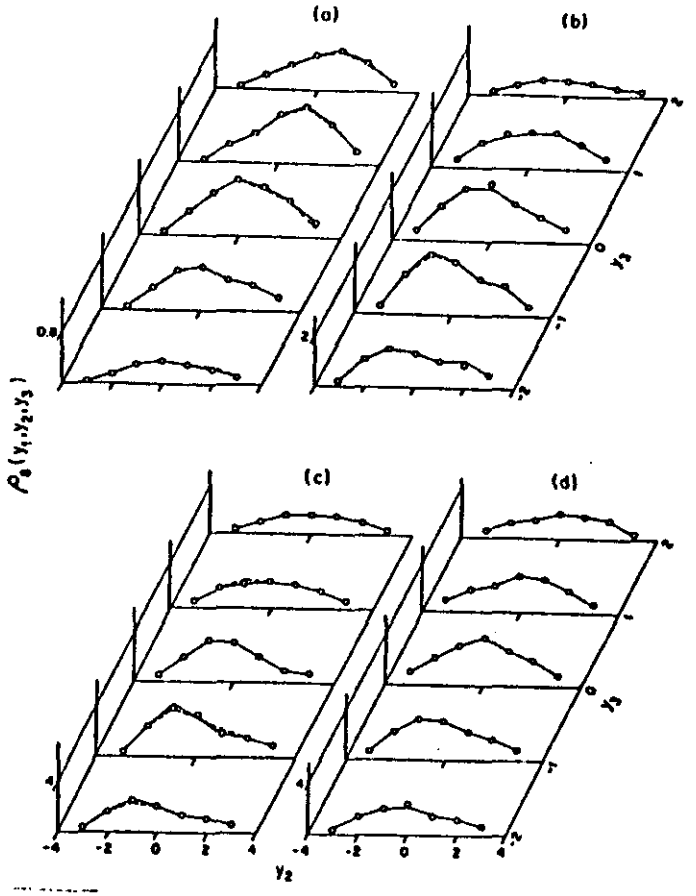

Fig. 14. The three-particle density function for 8-prong events from 200 GeV/c pp interactions. y_1 is fixed (±0.5 Units) at (a) -3, (b) -2, (c) -1, and (d) 0. The dashed (solid) curve represents the approximation of Eq. (7) (Eq. (8)).

$$\rho_n(1,2,3) = \frac{(n-1)(n-2)}{n^2}\ \rho_1^n(1)\ \rho_1^n(2)\ \rho_1^n(3) \tag{7}$$

$$+ (n-1)(n-2)\ [\rho_1^n(1)\ \tilde{C}_n(2,3) + \rho_1^n(2)\ \tilde{C}_n(3,1) + \rho_1^n(3)\ \tilde{C}_n(1,2)].$$

In addition, we have also tried the approximation

$$\rho_n(1,2,3) = \frac{\rho_2^n(1,2)\ \rho_2^n(2,3)\ \rho_2^n(3,1)}{\rho_1^n(1)\ \rho_1^n(2)\ \rho_1^n(3)} \cdot \frac{n(n-2)}{(n-1)^2}\,. \tag{8}$$

In Fig. 14 we show $\rho_8(1,2,3)$ with y_1 fixed at -3, -2, -1, and 0 while y_2, y_3 vary from -3 to 3. The approximations (7) and (8) are shown as the dashed and solid lines, respectively. It may be seen that both of these expressions represent the data reasonably well over a wide range of rapidity space.

We may now use (8) to construct[8] a general two-particle representation from which one may derive any distribution function for an n particle final state. Assume that

$$\frac{d\sigma_n}{dy_1 \ldots dy_n} = \prod_{i<j=1}^{n} f(y_i, y_j)\, F(Y), \text{ with } Y \sim \ln s,$$

$$\text{and let } f(y_i, y_j) = e^{-x(y_i, y_j)} .$$

$$\text{Then} \quad \sigma_n \rho_1^n(1) = \frac{1}{(n-1)!} \int dy_2 \ldots dy_n \prod_{i<j} f(y_i, y_j)\, F(Y), \text{ etc.}$$

Using Eq. (8) then leads to an integral equation for $\partial x/\partial y_1$ which can be solved for $x(y_1, y_2)$. The results are shown in Fig. 15 for four different charged multiplicities. The values for $x(y_1, y_2)$ are consistent with being independent of n. In addition, we have verified[8] that the function $x(y_1, y_2)$ correctly reproduces the density functions $\rho_1, \rho_2 \ldots$ An interesting feature of these plots is the appearance of the broad minimum at $y_1 = y_2$. This is a reflection of the short-range order observed in the two-particle correlation function.

IV. Rapidity Distribution Comparisons in $p^{\pm}p$, $\pi^{\pm}p \to \pi^{\pm}$

Data now exist[1] at 100 GeV/c for charged pion production in $\bar{p}p$, pp, π^+p and π^-p interactions. Using linear combinations of these distributions, we now present some preliminary attempts[9-11] to obtain information on the various components of multiparticle production, i.e., fragmentation, pionization and annihilation.

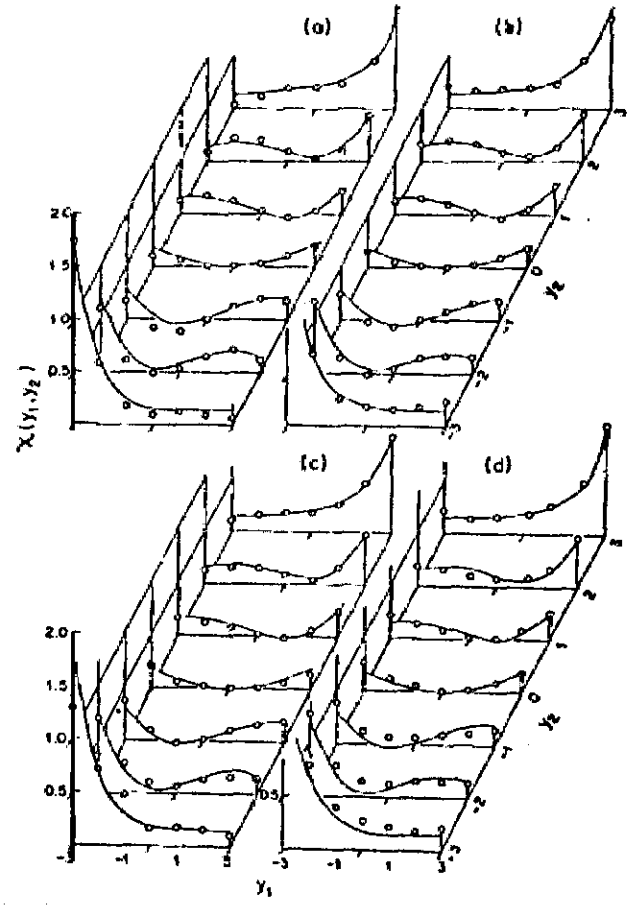

Fig. 15. The two-particle representation $x(y_1, y_2)$, see text, for (a) 6-, (b) 8-, (c) 10-, and (d) 12-prong events. The curve represents the average of 6-12 prong events.

In Ref. 5 we have shown that smooth extrapolations of the low energy annihilation multiplicity moments are obtained by estimating the high energy annihilation moments from the prescription

$$\sigma_n(\text{Ann}) = \sigma_n(\bar{p}p) - \sigma_n(pp) \equiv \Delta\sigma_n. \tag{9}$$

We now extend this to inclusive charged pion production ($\pi^c \equiv \pi^+ + \pi^-$):

$$\Delta_y(\pi^c) = \frac{d\sigma}{dy}(\bar{p}p \to \pi^c) - \frac{d\sigma}{dy}(pp \to \pi^c). \tag{10}$$

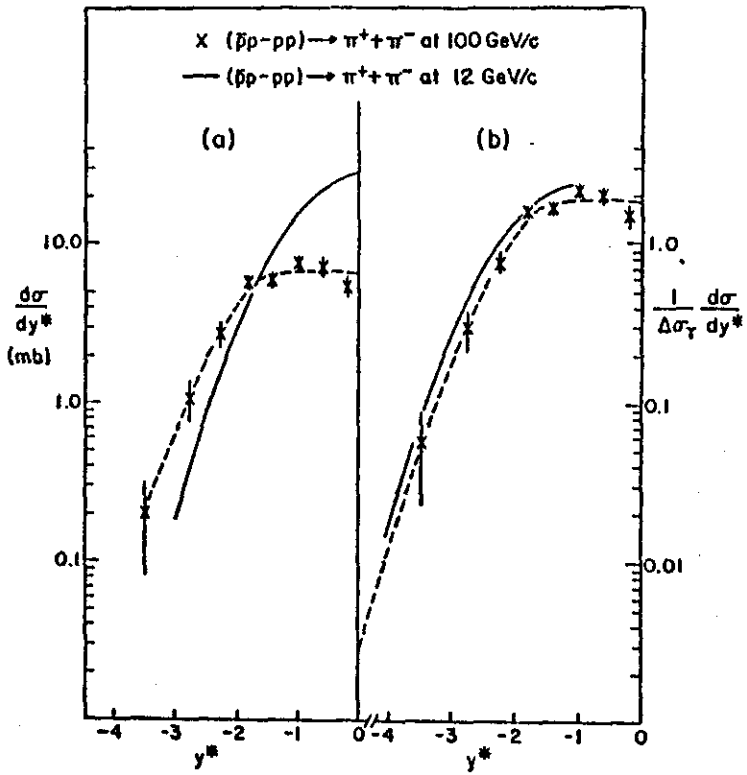

Fig. 16. (a) Rapidity spectra for the difference of $\pi^c \equiv \pi^+ + \pi^-$ production in $\bar{p}p$ and pp interactions at 12 and 100 GeV/c.
(b) as in (a) but normalized by the difference in $\bar{p}p$, pp total cross sections.

In Fig. 16(a) we show[9] $\Delta_y(\pi^c)$ at 12 and 100 GeV/c as a function of the CM rapidity. It is interesting to note[10], Fig. 16(b), that when each distribution is normalized by $\Delta\sigma_T = \sigma_T(\bar{p}p) - \sigma_T(pp)$, these data appear to scale rather well in the target fragmentation region.

To enhance the possibility of observing annihilation effects, we can study these differences as a function of the charged multiplicity of the final state. Figure 17 shows the ratio[9]

$$R_n(y) = \Delta_y^n(\pi^c)/\frac{d\sigma_n}{dy}\ (pp \to \pi^c) \qquad (11)$$

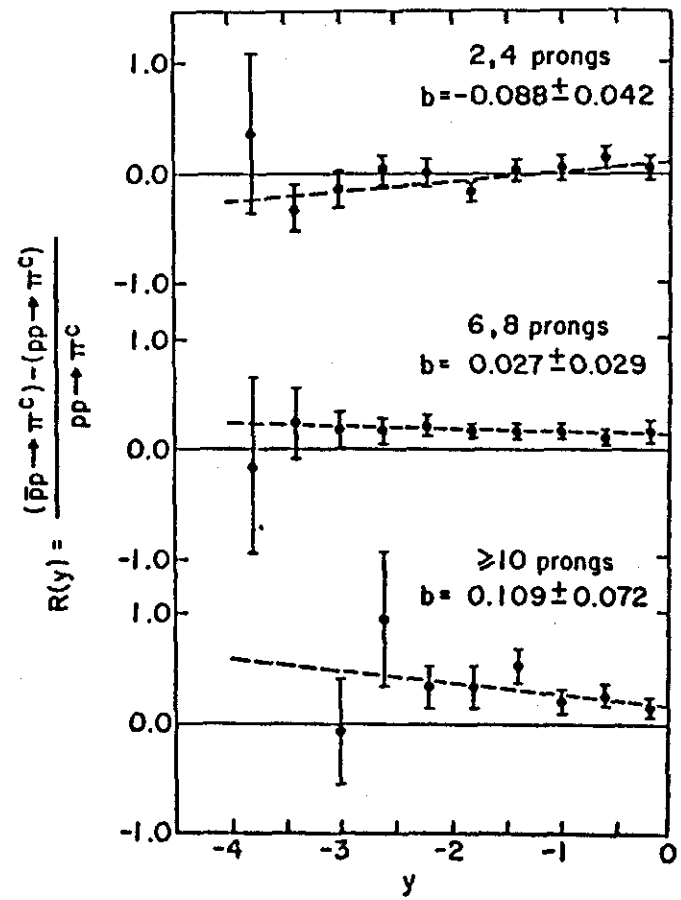

Fig. 17. Ratio $R_n(y)$ as a function of CM rapidity for different charged multiplicity final states. The dashed lines represent fits to the form $R = a + b|y|$.

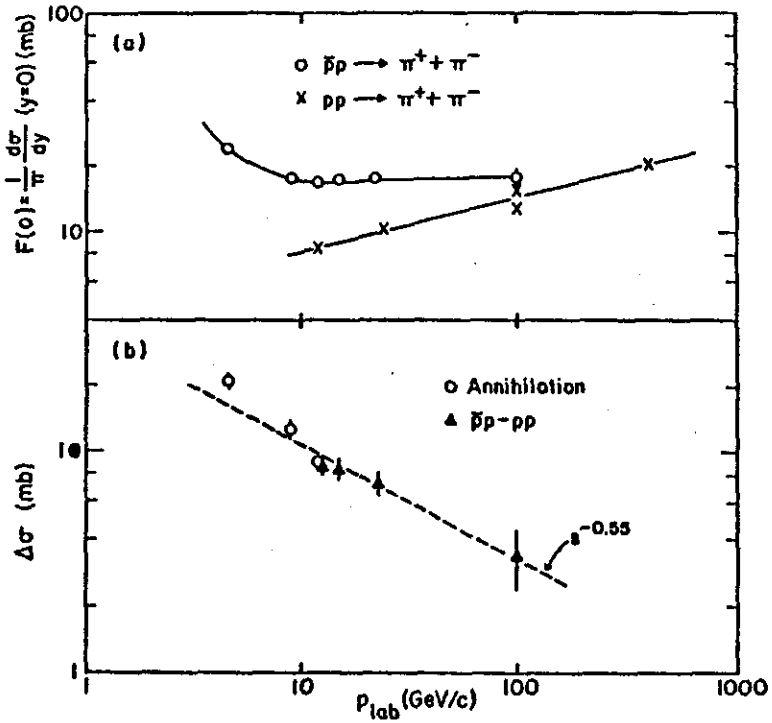

Fig. 18. (a) Values of $\frac{d\sigma}{dy}$ $(y^*=0)$ versus the incident beam momentum for $\pi^c \equiv \pi^+ + \pi^-$ in $p^\pm p$ interactions.
(b) Values of the differences $(\bar{p}p\text{-}pp)$ and the annihilation values at $y^*=0$.

as a function of the CM rapidity for three ranges of charged particle multiplicity. We note a tendency for the higher (lower) multiplicities to have a broader (narrower) rapidity spectrum than the nonannihilation final states.

The cross section differences in the central region may also be studied as a function of the CM energy, $\sqrt{s}$. It has been shown[10/] that $\Delta_y(y^*=0)$ should exhibit simple Mueller-Regge behavior due to ω-ω exchange and hence could be expected to display an $\sim s^{-0.55}$ dependence. In Fig. 18(a) we show a compilation of $\frac{d\sigma}{dy}$ $(y^*=0)$ for $p^\pm p \to \pi^c$ as a function of the incident beam momentum. In Fig. 18(b) we show the differences, $\Delta\sigma(y^*=0)$. The energy dependence of these data is in reasonable agreement with the Mueller-Regge expectation[10/] shown as a dashed line.

In an attempt to separate multiparticle production into four simple components (proton and pion fragmentation, a central pionization cloud and annihilation), we now consider[11/] linear combinations of the eight reactions at 100 GeV/c:

$$\bar{p}p \to \pi^\pm, \tag{12}$$

$$pp \to \pi^\pm, \tag{13}$$

$$\pi^+p \to \pi^\pm, \tag{14}$$

and

$$\pi^-p \to \pi^\pm. \tag{15}$$

We choose to normalize the rapidity distributions for reactions (12) to (15) by σ_{inel} at 100 GeV/c. Figure (19) shows the charge distributions for $\pi^\pm p$:

$$\frac{dQ}{dy} = \frac{1}{\sigma_{inel}}\left[\frac{d\sigma}{dy}(+) - \frac{d\sigma}{dy}(-)\right], \tag{16}$$

such that $\int \frac{dQ}{dy}\, dy = +2(0)$ for π^+p, pp (π^-p, $\bar{p}p$). Also shown for comparison are similar data at 16 GeV/c. We can now form linear combinations of these charge distributions (e.g., $\frac{1}{2}\left[\frac{dQ}{dy}(\pi^+p) \pm \frac{dQ}{dy}(\pi^-p)\right]$). To obtain a rather simple interpretation of the resulting spectra we now assume[11/] that

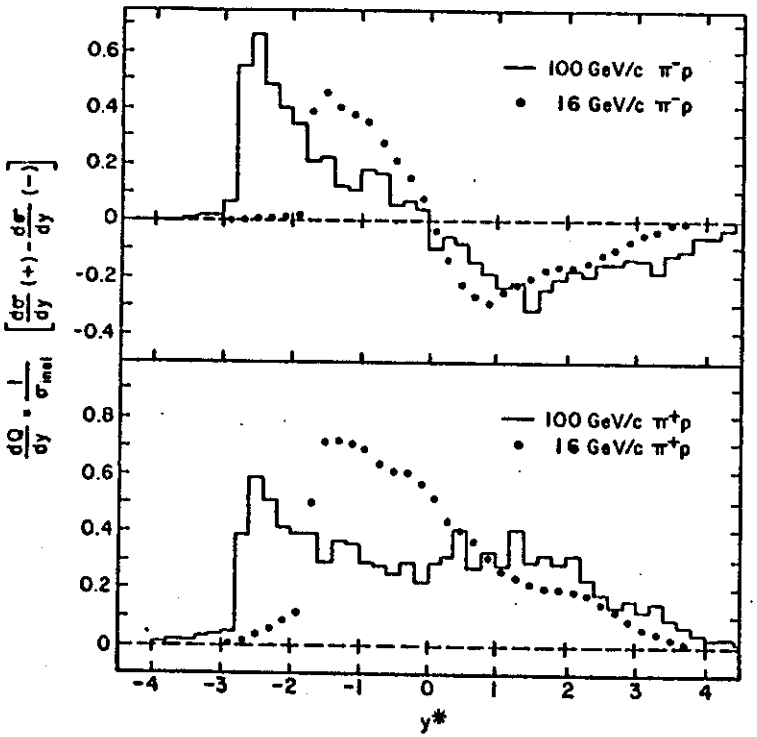

Fig. 19. Charge distributions for $\pi^{\pm}p$ interactions at 16 and 100 GeV/c.

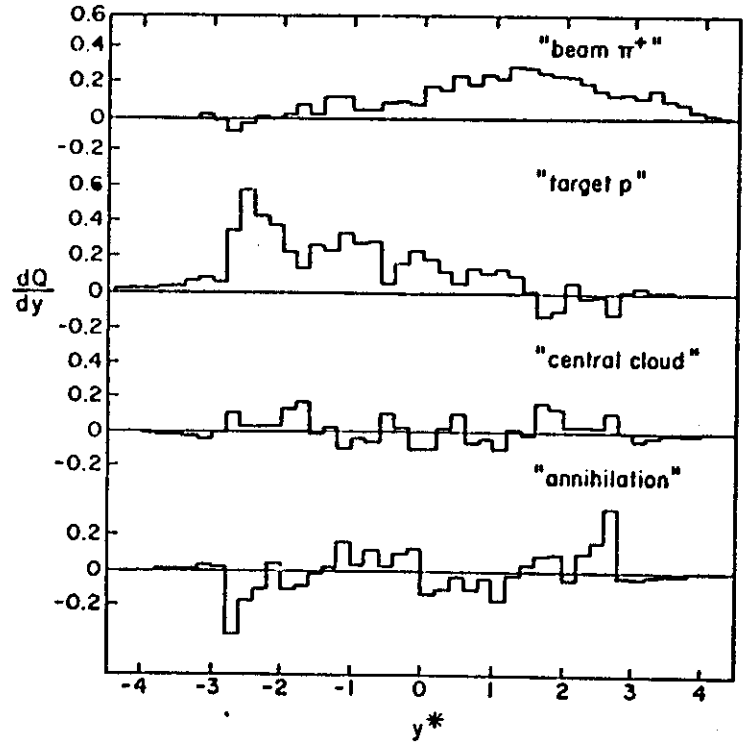

Fig. 20. Charge distributions for proton and pion fragmentation and central cloud and annihilation components at 100 GeV/c.

$$\pi^{\pm}p = (\text{target } p) + (\text{cloud}) + (\text{beam } \pi^{\pm}) \tag{17-18}$$

$$pp = (\text{target } p) + (\text{cloud}) + (\text{beam } p) \tag{19}$$

$$\bar{p}p = (\text{target } p) + (\text{cloud}) + (\text{annih.}) + (\text{beam } \bar{p}). \tag{20}$$

From these four relations, one can solve for the four noninterfering components. The results are shown in Fig. 20. We find that the proton and pion fragmentation components extend over a wide range in rapidity, that the pion cloud is essentially zero (as expected for a "cloud" with equal π^+ and π^- production), and that the annihilation component also is small. To determine the "true" extent of the cloud in rapidity space, we now use Eqs. (17) to (20) for π^+ and π^- production separately (as opposed to

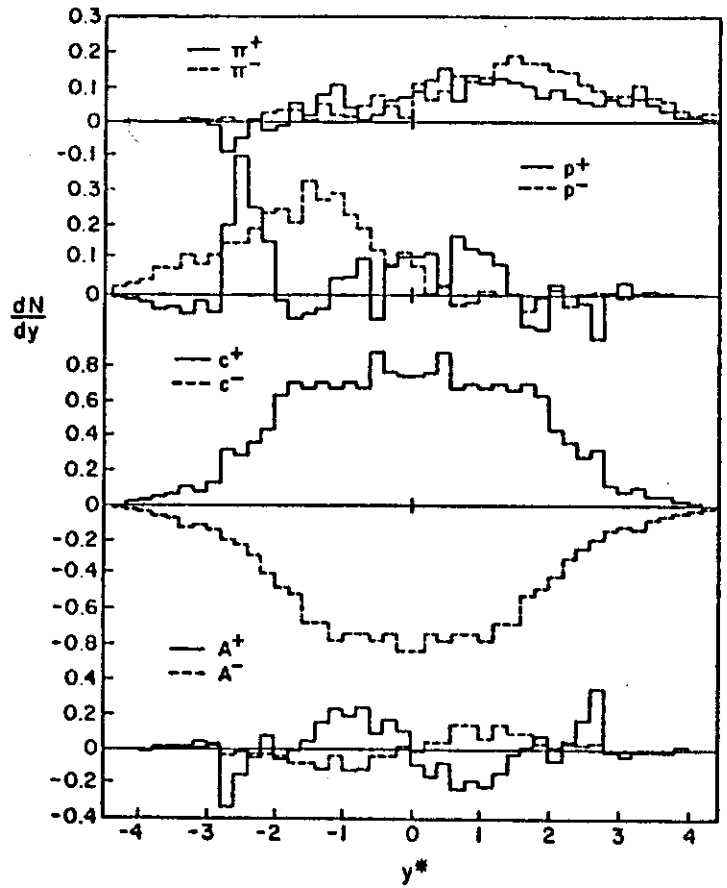

Fig. 21. Rapidity spectra for the positively and negatively charged contributions to the proton and pion fragmentation and central cloud and annihilation components at 100 GeV/c.

the net charge which is the difference of the two). The results shown in Fig. 21 now indicate that the pion cloud is a dominant contribution to the production process for charged pions. Finally, we note that the pion cloud rapidity spectrum exhibits a remarkably wide plateau (∿ ±2 units) which is not apparent in the raw distributions for reactions (12) - (15).

ACKNOWLEDGMENT

It is a pleasure to acknowledge discussions with A. Erwin, B. Oh, M. Pratap, and G. Smith.

REFERENCES

* Work supported in part by the National Science Foundation.

1. J. Whitmore, Phys. Rep. 27C, 187 (1976).
2. P. Stix and T. Ferbel, submitted to Phys. Rev. D (1976).
3. C. Bromberg et al.,Phys. Rev. Lett 31, 1563 (1973).
4. A. Firestone et al., to be published in Phys. Rev. D (1976).
5. J. G. Rushbrooke et al., Phys. Letters 59B, 303 (1976).
6. B. Y. Oh et al., Nucl. Phys. B, to be published (1976).
7. V. P. Kenney et al., Paper submitted to Inter. Conf. on High Energy Physics, Tbilisi, U.S.S.R. (1976).
8. M. Pratap et al., Nucl. Phys. B, to be published (1976).
9. J. Whitmore et al., Properties of Inclusive $\pi^{\pm}$ production in 100 GeV/c Antiproton-proton Interactions, paper in preparation.
10. J. G. Rushbrooke, High Energy Antinucleon-Nucleon Annihilation Interactions, in Proc. of the Symposium on $\bar{N}N$ Interactions, Stockholm, 1976.
11. A. Erwin, Private communication and paper in preparation.